Enhanced Photoactivity with Nanocluster-Grafted Titanium Dioxide Photocatalysts

Min Liu,[‡] Ryota Inde,[†] Masami Nishikawa,[⊥] Xiaoqing Qiu,[‡] Daiki Atarashi,[†] Etsuo Sakai,[†] Yoshio Nosaka,[⊥] Kazuhito Hashimoto,[‡,§,*] and Masahiro Miyauchi[†,∥,*]

[†]Department of Metallurgy and Ceramics Science, Graduate School of Science and Engineering, Tokyo Institute of Technology, 2-12-1 Ookayama, Meguro-ku, Tokyo 152-8552, Japan, [‡]Research Center for Advanced Science and Technology, The University of Tokyo, 4-6-1 Komaba, Meguro-ku, Tokyo 153-8904, Japan, [§]Graduate School of Engineering, The University of Tokyo, 7-3-1 Hongo, Bunkyo-ku, Tokyo 113-8656, Japan, [⊥]Department of Materials Science and Technology, Nagaoka University of Technology, 1603-1, Kamitomioka-machi, Nagaoka, Niigata 940-2188, Japan, and [∥]Japan Science and Technology Agency (JST), PRESTO, 4-1-8 Honcho Kawaguchi, Saitama 332-0012, Japan

ABSTRACT Titanium dioxide (TiO_2), as an excellent photocatalyst, has been intensively investigated and widely used in environmental purification. However, the wide band gap of TiO_2 and rapid recombination of photogenerated charge carriers significantly limit its overall photocatalytic efficiency. Here, efficient visible-light-active photocatalysts were developed on the basis of TiO_2 modified with two ubiquitous nanoclusters. In this photocatalytic system, amorphous Ti(IV) oxide nanoclusters were demonstrated to act as hole-trapping centers on the surface of TiO_2 to efficiently oxidize organic contaminants, while amorphous Fe(III) or Cu(II) oxide nanoclusters mediate the reduction of oxygen molecules. Ti(IV) and Fe(III) nanoclusters-modified TiO_2 exhibited the highest quantum efficiency (QE = 92.2%) and reaction rate (0.69 μmol/h) for 2-propanol decomposition among previously reported photocatalysts, even under visible-light irradiation (420−530 nm). The desirable properties of efficient photocatalytic performance with high stability under visible light with safe and ubiquitous elements composition enable these catalysts feasible for large-scale practical applications.

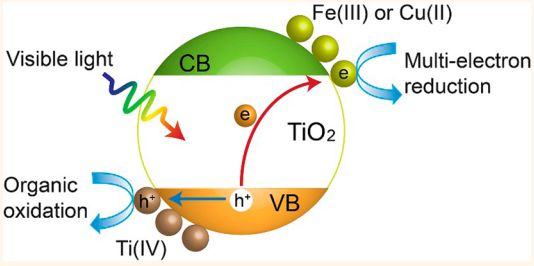

KEYWORDS: TiO_2 · nanocluster · visible light · photocatalysis · high quantum efficiency

The development of a safe, abundant and inexpensive photocatalyst is a significant consideration in solving the current energy and environmental issues.[1−6] Titanium dioxide (TiO_2) is one of the promising materials because of its nontoxic, resource abundant, chemically stable properties, and has therefore attracted a great deal of attention for the applications in water splitting, decomposition organic pollutants, solar cells and so on.[7−11] However, TiO_2 has a wide band gap and can only be activated under ultraviolet (UV) light irradiation, which limits its practical applications. To effectively utilize solar light and indoor light, the doping of TiO_2 with various transition metal cations and anions has been extensively investigated to extend its light absorption to visible light region.[12−20] Although most systems doped in this way can show visible light absorption, these systems are still unsatisfactory for practical use, because their quantum efficiencies (QEs) under visible light are much lower than those under UV light.[21] This limit is mainly arisen from that the dopants generate impurity and/or vacancy levels in the band gap, which serve as the recombination centers for the photogenerated charge carriers.[12−21] As an alternative, Kisch *et al.* developed the photosensitization of TiO_2 by surface modification with platinum(IV) chloride.[22] The development of photocatalyst by surface modification process is very attractive because the visible-light activity can be induced by the simple process without introduction of impurity or vacancy levels into crystal. TiO_2 grafted with some transition metal oxide nanoclusters, such as Fe(III) or Cu(II) nanoclusters, are also capable of serving as visible-light sensitive photocatalysts.[23−27] When Fe(III) or Cu(II) nanoclusters were grafted onto the surface of TiO_2, electrons in the valence band (VB)

* Address correspondence to mmiyauchi@ceram.titech.ac.jp, hashimoto@light.t.u-tokyo.ac.jp.

Received for review April 24, 2014 and accepted June 2, 2014.

Published online June 02, 2014
10.1021/nn502247x

of TiO_2 can be excited to these clusters *via* an interfacial charge transfer (IFCT) process under visible light irradiation.[28,29] In addition, these clusters can mediate the multielectron reduction of oxygen molecules.[30−35] The QE of these systems have already exceeded 20%. Under this condition, the oxidation reactivity caused by photogenerated holes limits the photocatalytic performance, while the QE of the reduction reaction is sufficiently high because of the efficient electron reduction of oxygen. Therefore, the next challenge for improving the photocatalytic properties under visible light is to promote the oxidation reaction of holes. To date, various noble metal oxide nanoclusters, such as RuO_2, IrO_2 and so on,[36−44] have been widely used as the cocatalysts for hole trapping centers, even though some other nanoclusters such as cobalt phosphate can also show good performances for hole trapping.[45] However, the use of noble metals like Pt, Ir, or Ru is not economical and extremely limits the possibility for practical applications. Rare metals in natural resource are limited; thus, the concept of "ubiquitous strategy" becomes more important and essential for the industrial activities.[46] Ubiquitous means existing or being everywhere especially at the same time, and the development of photocatalyst by a nontoxic and economical resources is indispensable for the recent practical applications.

In the present paper, we propose the three important requirements to develop the visible-light-sensitive photocatalysts by the modification of hole trapping centers on the semiconductor photocatalysts; (1) both semiconductor photocatalysts and hole trapping centers are composed of ubiquitous elements (nontoxic and economical elements), (2) the occupied electronic states of hole trapping centers are more negative than those of semiconductor photocatalyst, (3) synthesis of these hole trapping centers should be facile. Recent studies indicated that the interface bonding between semiconductors and clusters influenced their electronic structure.[47] In case of TiO_2, bonding length between Ti(IV) cation and oxygen anion in bulk is different from that in surface specific cluster's site, and the holes in these specific surface sites are more stable than those in bulk.[47,48] Consequently, the recent study indicated that the specific Ti(IV) sites on the bulk TiO_2 could act as efficient hole trapping centers.[48] However, the generation of these specific sites on the surface of rutile TiO_2 in the previous report involved a complicated processes of reduction in a vacuum followed by oxidation in an oxygen atmosphere at elevated temperatures,[48] which largely decrease their practical applicable. Herein, we demonstrate that the amorphous Ti(IV) oxide nanoclusters grafted on the surface of TiO_2 by a simple impregnation method can serve as efficient hole trapping centers. By further grafting of Fe(III) or Cu(II) nanoclusters onto TiO_2, a highly visible-light-active TiO_2 photocatalysts with the highest QE and reaction rate among the reported visible-light sensitive photocatalystshave been achieved for decomposing 2-propanol (IPA) under visible-light (420−530 nm) irradiation.

RESULTS AND DISCUSSION

Ti(IV) Nanoclusters Grafted on Rutile TiO_2 as Hole Trapping Centers. To investigate the work function with grand state of Ti(IV) nanoclusters onto bulk TiO_2, kelvin probe force microscope (KPFM) analysis was conducted on the Ti(IV) nanoclusters grafted rutile single crystals in the dark condition. The Ti(IV) nanoclusters were grafted on the rutile TiO_2 single crystals with (110) face by a simple impregnation method. Topographic images (Figure 1a and Figure S1, Supporting Information) clearly show that Ti(IV) nanoclusters were successfully grafted on the smooth surface of TiO_2 single crystals. Figure 1b shows the KPFM image of the Ti(IV) nanoclusters grafted TiO_2 (Ti(IV)−TiO_2) single crystals in the dark condition. It can be clearly seen that the potential of Ti(IV) nanoclusters is more negative than that of rutile bulk TiO_2, indicating that the work function of Ti(IV) clusters is smaller than that of bulk TiO_2 under their grand states.[49−51] Both the bulk TiO_2 and Ti(IV) clusters are n-type semiconductors, thus their Fermi-levels lie under the conduction band. The KPFM results indicate that the conduction band of Ti(IV) clusters is more negative than that of bulk TiO_2. Next, we examined the excited states of Ti(IV)−TiO_2 single crystals by observing photocatalytic probing reaction. As probe reactions, the photocatalytic oxidation of $Pb(NO_3)_2$ (1) by Ti(IV)−TiO_2 single crystals was conducted under UV light (300−400 nm) irradiation (Figure S2, Supporting Information).[52−54]

$$Pb^{2+} + 2H_2O + 2h^+ \rightarrow PbO_2 + 4H^+ \qquad (1)$$

It can be seen that PbO_2 can be deposited on both bare and Ti(IV)−TiO_2 single crystals (Figure 1c,d), indicating the TiO_2 can be effectively activated under UV light irradiation. However, only limited PbO_2 clusters were deposited on the surface of the bare TiO_2 single crystals, showing that the charge separation efficiency on bare single crystals is rather low. In contrast, after Ti(IV) nanoclsuters grafting, large amount of PbO_2 clusters can be obviously observed on the surface of Ti(IV)−TiO_2 single crystals, indicating that the density of photogenerated holes on the surface was drastically enhanced after Ti(IV) nanoclusters grafting.

To investigate the excited species by spectroscopic analysis, electron spin resonance (ESR) spectra for Ti(IV) grafted rutile TiO_2 powder and bare rutile powder were recorded under UV light irradiation (Figure S3, Supporting Information). Both samples showed ESR signals at $g_1 = 2.030$, $g_2 = 2.011$ and $g_3 = 2.004$, which are assigned to the surface trapped holes according to the previous reports.[55−57] Notably, the ESR signal at g_2 of Ti(IV)−TiO_2 was more obvious than that of bare TiO_2.

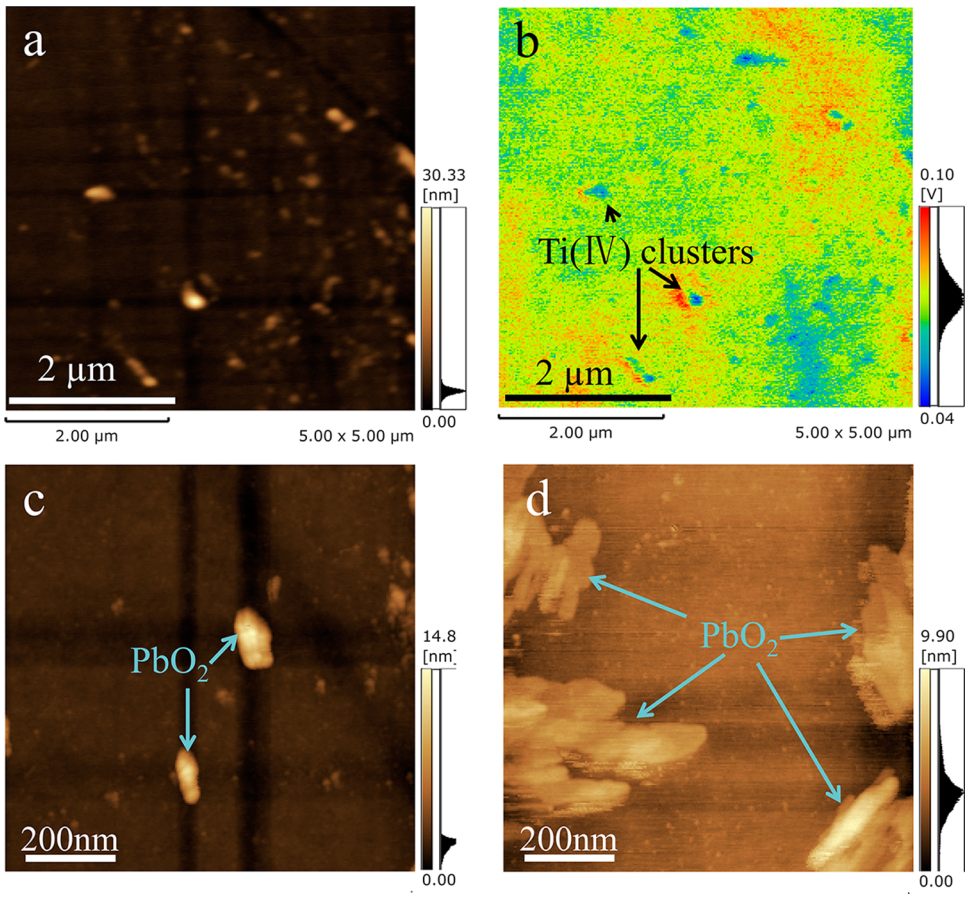

Figure 1. (a) Topographic AFM image of Ti(IV)−TiO_2 single crystal. (b) The corresponding KPFM image of Ti(IV)−TiO_2 single crystal in (a). (c) Topographic AFM image of PbO_2 deposited TiO_2 single crystal and (d) AFM image of PbO_2 deposited Ti(IV)−TiO_2 single crystal.

Furthermore, additional small signal at $g_1 = 2.028$ was observed on the Ti(IV)−TiO_2. These signals are assigned to the holes trapped at surface oxygen anion radicals or hydroxyl radicals such as $Ti^{4+}O\cdot^{-}Ti^{4+}OH^{-}$ or $OH\cdot$,[58−61] indicating that the photogenerated holes are trapped in Ti(IV) clusters under UV irradiation. The recent theoretical study indicated that both conduction and valence bands of sub 1 nm Ti(IV) clusters supported on rutile crystal are more negative than those of bulk rutile TiO_2, even though the sub 1 nm Ti(IV) clusters cause the band gap widening by quantum size effect.[47] The terminal oxygen atoms in these clusters contribute to shift of the valence band.[47] Also, recent evidence indicates that the specific surface clusters, such as the surface oxygen centered anion with two coordinating titanium ions, are potential sites for trapping photogenerated holes.[48] These reports also indicate that the bonding distance between neighboring Ti and O ions is very important to generate hole trapping sites. In the present study, the grafting of Ti(IV) was conducted by a hydrolysis of an aqueous $TiCl_4$ solution; thus, the oxygen ions dissociatively react with titanium ions to form the clusters. Because the coordination of the titanium ion in these clusters is different from that in bulk TiO_2, specific Ti(IV) sites were probably formed in the nanoclusters and at the interface between nanoclusters and bulk rutile TiO_2. Therefore, our Ti(IV) clusters act as hole trapping sites, which play a key role in the photoxidation reactions. Our Supporting Information revealed that the grafting of Ti(IV) clusters on bare TiO_2 nanoparticles greatly improved photocatalytic activities for both anatase and rutile cases without affecting their basic physicochemical properties, such as crystal structure, light absorption, morphology and so on (Figure S4−S7, Supporting Information). Further, we grafted Ti(IV) nanoclusters on the TiO_2 surface *via* a facile impregnation method, whereas the generation of these specific sites on the surface of rutile TiO_2 in the previous report involved a complicated processes.[48] The facile method facilitates the usefulness of Ti(IV) nanoclusters in various photocatalysts and photocatalytic systems.

Ti(IV) and Fe(III) or Cu(II) Nanoclusters Grafted TiO_2 Nanocomposites and Their Photocatalytic Activities. TiO_2 nanocomposites cografted with Ti(IV) and Fe(III) or Cu(II) nanoclusters (denoted as Fe(III)−Ti(IV)−TiO_2 and Cu(II)−Ti(IV)−TiO_2, respectively) were prepared using a simple two-step impregnation method (Figure S8, Supporting Information). Figure 2 shows a transmission electron microscope (TEM) image and the results

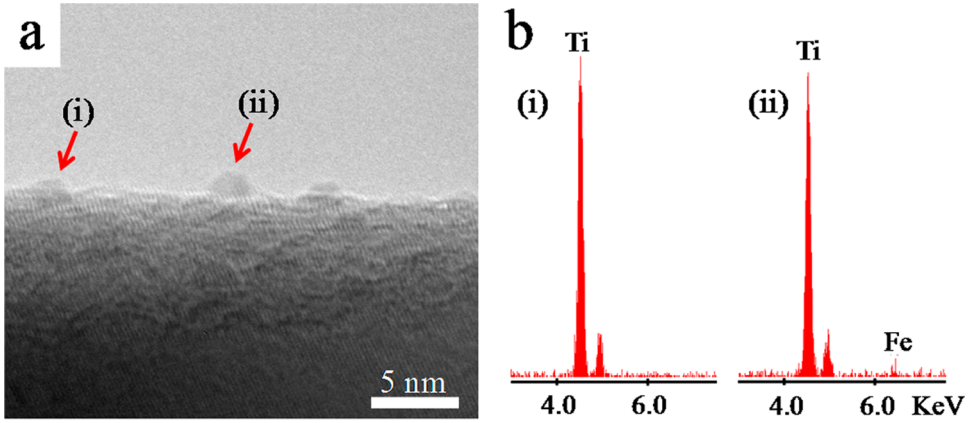

Figure 2. TEM and point EDS analyses of Fe(III)−Ti(IV)−TiO_2 nanocomposites. (a) TEM image of the Fe(III)−Ti(IV)−TiO_2 nanocomposite. (b) Point EDS spectra of the Fe(III)−Ti(IV)−TiO_2 nanocomposite. The spectra correspond to the points indicated in the TEM image.

of point energy dispersive X-ray spectroscopy (EDS) analysis for the Fe(III)−Ti(IV)−TiO_2 nanocomposite. The TEM analysis revealed that both Fe(III) and Ti(IV) clusters were deposited on the surface of rutile TiO_2 particles. The two types of clusters were less than 3 nm in size and were highly dispersed on the TiO_2 surface. X-ray diffraction (XRD; Figure S9, Supporting Information), X-ray photoelectron spectroscopy (XPS, Figure S10, Supporting Information), scanning electron microscopy (SEM; Figure S11, Supporting Information), and Brunauer−Emmett−Teller (BET; Table S1, Supporting Information) surface area analyses showed that the grafting of Ti(IV) and Fe(III) nanoclusters did not alter the crystallinity, morphology, or surface area of TiO_2. UV−vis spectra (Figure S12, Supporting Information) also revealed that grafting of Ti(IV) nanoclusters did not affect light absorption by TiO_2. However, after the grafting of Fe(III) nanoclusters onto the Ti(IV)−TiO_2 nanocomposite, clear visible-light absorption, which was attributed to IFCT absorption,[28,29] was observed. XPS, XRD, UV−vis spectra and SEM analyses confirmed that the Cu(II)−Ti(IV)−TiO_2 and Fe(III)−Ti(IV)−TiO_2 nanocomposites had similar structures and physicochemical properties (Figure S13−S16, Supporting Information).

According to the previous X-ray absorption fine structure (XAFS) analysis, Cu(II) clusters on the surface of TiO_2 has a distorted CuO structure, in which the apical oxygen approaches the Cu(II), forming the five-coordinate square pyramid.[24] Regarding the Ti(IV) clusters, theoretical studies indicated that oxygen atoms of metal oxide clusters on the TiO_2 surface could bind to 5-fold coordinated surface Ti atoms.[47] Thus, these amorphous clusters connect with the TiO_2 surface through the binding of oxygen atoms of clusters with 5-fold coordinated surface Ti atoms.[24,25,47] Further, the roles of Cu(II) and Fe(III) clusters have been thoroughly investigated by spectroscopic and chemical-probe analyses,[34,35] which have shown that the electrons in the VB of TiO_2 are excited to the Cu(II) or Fe(III) clusters by an IFCT process. Irie *et al.*[24] also investigated the role of Cu(II) nanoclusters as electron-trapping by *in situ* XAFS analysis performed under visible-light in the presence of IPA and absence of oxygen. Although Cu(I) was generated under these conditions, it converted back to Cu(II) upon exposure to oxygen, indicating that Cu(I) has oxygen reduction activity. Similar study was also conducted on the role of Fe(III) nanoclusters.[25] These results clearly indicate that Cu(II) and Fe(III) nanoclusters are efficient cocatalysts for electron trapping and multielectron reduction reactions. Importantly, the chemical state and environment of surface Cu(II) and Fe(III) nanoclusters in the present Cu(II)−Ti(IV)−TiO_2 and Fe(III)−Ti(IV)−TiO_2 samples are similar to those of the previous Cu(II)−TiO_2 and Fe(III)−TiO_2 systems. Thus, Cu(II) and Fe(III) nanoclusters in the present Cu(II)−Ti(IV)−TiO_2 and Fe(III)−Ti(IV)−TiO_2 function as identical roles as efficient cocatalysts for electron trapping and multielectron reduction reactions as in previous Cu(II)−TiO_2 and Fe(III)−TiO_2 systems.

The photocatalytic activities of the prepared nanocomposites were evaluated by measuring the decomposition of gaseous 2-propanol (IPA) under visible-light irradiation at 420−530 nm. The light intensity in the analysis was 1.0 mW/cm^2 (Figure S17, Supporting Information), which corresponded to an illuminance of 300 lx and was comparable to the intensity of regular indoor lighting, such as white fluorescent bulbs and light-emitting diodes (LED). A typical profile of the decomposition of IPA into the final product CO_2 *via* the intermediary product acetone for the Fe(III)−Ti(IV)−TiO_2 nanocomposite is shown in Figure 3a. After ~30 h of irradiation, the concentration of CO_2 generated by Fe(III)−Ti(IV)−TiO_2 reached approximately 900 ppmv (~18 μmol), which is nearly 3 times the amount of IPA initially injected into the vessel (300 ppmv), indicating that IPA was completely decomposed. Notably, CO_2 generation over bare TiO_2 and Ti(IV)−TiO_2 was negligible (Figure 3b) as these materials

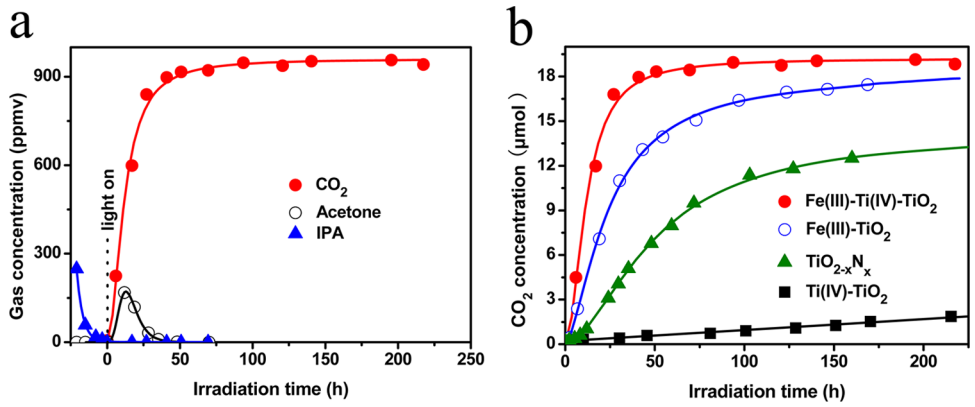

Figure 3. Photocatalytic performance of the Fe(III)−Ti(IV)−TiO_2 nanocomposites. (a) Representative time-dependent gas concentrations during IPA decomposition over Fe(III)−Ti(IV)−TiO_2. (b) Comparative analysis of CO_2 generation over Ti(IV)−TiO_2, $TiO_{2-x}N_x$, Fe(III)−TiO_2 and Fe(III)−Ti(IV)−TiO_2.

TABLE 1. Photocatalytic Performances of Photocatalysts[a]

sample	$TiO_{2-x}N_x$	Cu(II)−TiO_2	Cu(II)−Ti(IV)−TiO_2	Fe(III)−TiO_2	Fe(III)−Ti(IV) TiO_2
R^i_p (quanta/sec)	1.30×10^{16}	1.30×10^{16}	1.30×10^{16}	1.30×10^{16}	1.30×10^{16}
R^a_p (quanta/sec)	4.10×10^{15}	4.69×10^{14}	4.69×10^{14}	7.48×10^{14}	7.48×10^{14}
R_{CO_2} (μmol/h)	0.16	0.13	0.42	0.40	0.69
QE (%)	3.9	27.7	89.6	53.5	92.2

[a] R^i_p, rate of incident photons; R^a_p, absorbed photon numbers in photocatalysts; R_{CO_2}, CO_2 generation rate; QE, quantum efficiency.

do not absorb visible light (Figure S6, Supporting Information).

The Fe(III)−TiO_2 nanocomposite was active under visible-light due to the Fe(III) nanoclusters, which mediated the efficient IFCT and multielectron reduction reactions.[25] However, over 100 h was required for IPA to be completely decomposed, and the visible-light activity of Fe(III)−TiO_2 was lower than that of the Fe(III)−Ti(IV)−TiO_2 nanocomposite, although both materials had almost identical physicochemical properties, including crystallinities and surface areas. Comparatively, $TiO_{2-x}N_x$, which is recognized as an efficient visible-light photocatalyst,[12] required over 300 h to completely decompose gaseous IPA. The limited efficiency of $TiO_{2-x}N_x$ is due to the lower oxidation power of the photogenerated holes in nitrogen levels than those in the VB.[21] For Cu(II)−Ti(IV)−TiO_2 nanocomposites (Figure S18, Supporting Information), in contrast, the cografting of Ti(IV) and Cu(II) nanoclusters on the TiO_2 surface also drastically enhanced visible-light photocatalytic performance compared with that of Cu(II)−TiO_2 and $TiO_{2-x}N_x$, which exhibited similar photocatalytic activities. After Ti(IV) nanoclusters were grafted onto Cu(II)−TiO_2, the photocatalytic activity of the obtained Cu(II)−Ti(IV)−TiO_2 nanocomposites was increased approximately three fold compared to that of $TiO_{2-x}N_x$.

On the basis of the observed photocatalytic activities, the QE for CO_2 generation by the prepared photocatalysts was calculated using the following equation: QE = $R^r_p/R^a_p = 6R_{CO_2}/R^a_p$, where R^r_p is the reaction rate of photons involved in CO_2 generation, R_{CO_2} is the CO_2 generation rate, and R^a_p is the absorption rate of incident photons. The details of this calculation are described in the literature[12] and the Supporting Information (Figure S19). The calculated data are summarized in Table 1. The QE for CO_2 generation by Fe(III)−Ti(IV)−TiO_2 was 92.2%, which is the highest value among the previously reported visible-light photocatalysts. This QE is much higher than that of P25 TiO_2 nanoparticles under UV light irradiation, which is widely considered as one of the most efficient UV-light-active photocatalysts.[27] The CO_2 generation rate (R) of our Fe(III)−Ti(IV)−TiO_2 was estimated to be 0.69 μmol/h, which is one of the highest R for visible-light photocatalysts reported to date.[27]

The photocatalytic activity of the developed nanocomposites was also found to be dependent on the loading amount of Ti(IV) nanoclusters (Figure S20, Supporting Information). The optimal loading amount of Ti(IV) clusters to achieve the high photocatalytic activity was 0.25 wt % for both Cu(II)- and Fe(III)-grafted TiO_2. Notably, under optimal loading conditions, further grafting Ti(IV) nanoclusters on the surface of Cu(II)−TiO_2 enhanced the QE from 27.7 to 89.6%. Further, we demonstrated that the high performance of these Fe(III)−Ti(IV)−TiO_2 and Cu(II)−Ti(IV)−TiO_2 could be maintained under repeated light irradiation in air for one year (Figure S21, Supporting Information), and estimated that the turnover number of this system exceeded 80. The Fe(III)−Ti(IV)−TiO_2 and Cu(II)−Ti(IV)−TiO_2 samples were also very active under

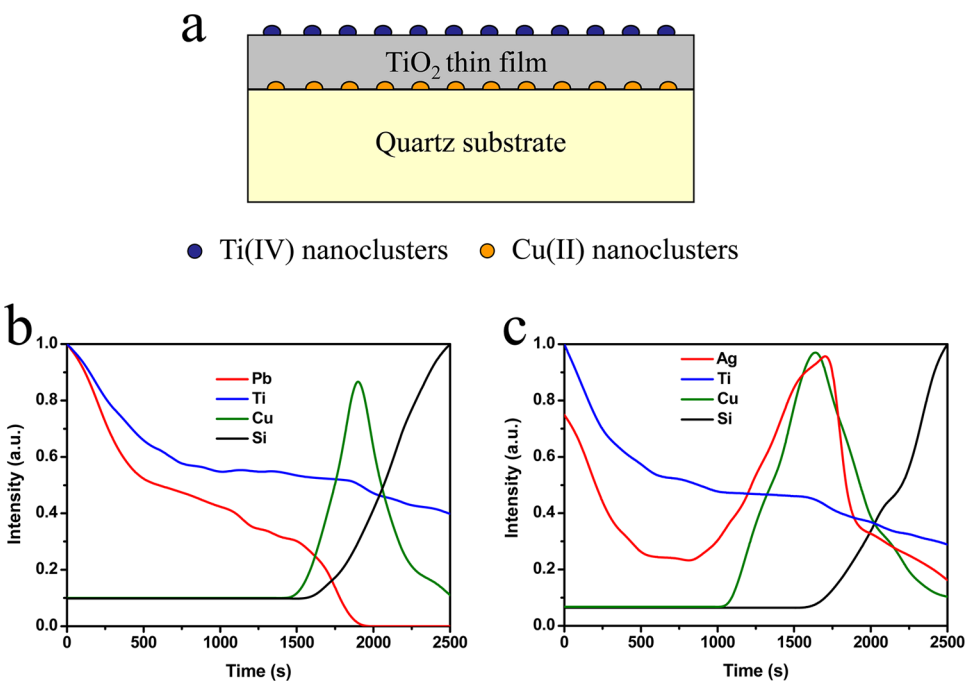

Figure 4. Depth profiles of metal or metal oxide deposited Ti(IV)/TiO_2/Cu(II) thin film. (a) Schematic image of the Ti(IV)/TiO_2/Cu(II) thin film. (b) Normalized distribution of Ti, Pb, Cu and Si in Cu(II)/TiO_2/Ti(IV) thin film after oxidation of lead nitrate. (c) Normalized distribution of Ti, Ag, Cu, and Si in Cu(II)/TiO_2/Ti(IV) thin film after reduction of silver nitrate.

UV-light irradiation. Thus, we can safely conclude that our photocatalysts have high photocatalytic activity with high stability, indicating their great potential for practical applications.

Charge Transfer Processes under Visible Light Irradiation. Next, to investigate the visible light excitation process, we prepared Ti(IV) and Cu(II) nanoclusters modified TiO_2 (Ti(IV)/TiO_2/Cu(II)) thin films (Figures 4a, S22 and S23, Supporting Information) and examined the charge transfer processes in the thin films by observing photodeposited particles under visible light. As probe reactions, the photocatalytic oxidation of $Pb(NO_3)_2$ (1) and photocatalytic reduction of $AgNO_3$ (2) by Ti(IV)/TiO_2/Cu(II) thin film were conducted under visible-light (420−530 nm) irradiation.[52−54]

$$Ag^+ + e^- \rightarrow Ag \qquad (2)$$

On the basis of these reactions, we can determine the active sites for the electron trapping and hole trapping by observing photodeposited particles. To investigate the distribution of photodeposited PbO_2 and Ag particles in the prepared thin films, the elemental depth profiles of the Ti(IV)/TiO_2/Cu(II) thin film were recorded by XPS using Ar^+ ion etching, as shown in Figure 4b,c. The normalized elements distribution in Figure 4b clearly shows that the Pb signal was mainly found in the close vicinity of the thin film surface. Notably, the Pb signal disappeared when the Cu(II) signal appeared at the bottom of the thin film, where the Si signal was drastically enhanced, indicating that the photogenerated holes did not accumulate at the sites of Cu(II) nanoclusters. We also investigated amount of PbO_2 on the TiO_2/Cu(II) thin film and found that a smaller number of PbO_2 particles were deposited on the surface compared to that on the Ti(IV)/TiO_2/Cu(II) thin film (Figure S24, Supporting Information). Therefore, the results suggested that holes mainly accumulated on the thin film surface where Ti(IV) nanoclusters were grafted.

It is possible to consider that the efficient PbO_2 deposition might be due to the high surface area and/or adsorbability on Ti(IV) clusters. However, the intensities of Pb signals under the dark condition were similar between TiO_2/Cu(II) and Ti(IV)/TiO_2/Cu(II) thin films, indicating that the adsorption of Pb species in the dark is almost the same between Ti(IV)−TiO_2 and TiO_2 (Figure S25, Supporting Information). We also measured the zeta potentials of powders under the neutral aqueous condition, and those of Ti(IV)−TiO_2 and pure TiO_2 were −19 and −13 mV, respectively. These zeta potentials difference was only 6 mV with very close value, indicating the similar adsorbabilities for ionic substances. Further, ESR spectra for Ti(IV)−TiO_2−Cu(II) and TiO_2−Cu(II) nanocomposites were investigated under visible light irradiation (Figure S26, Supporting Information), and the results strongly supports the hole trapping in the Ti(IV) nanoclusters. On the basis of these experimental results, we can conclude that the efficient PbO_2 deposition onto the Ti(IV) nanoclusters is due to the hole trapping effect, rather than the adsorbability.

On the other hand, the depth profile of the Ti(IV)/TiO_2/Cu(II) thin film after reduction of silver nitrate shows that Ag particles were mainly deposited at the

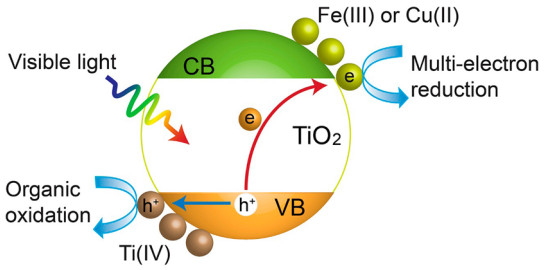

Figure 5. Proposed photocatalysis processes.

sites of Cu(II) nanoclusters. Surface XPS spectra were also recorded after Ag deposition under visible light irradiation (Figure S27, Supporting Information), and the amount of Ag deposition on the Ti(IV)/TiO_2/Cu(II) thin film was much smaller than that on the TiO_2/Cu(II) film. These results also indicate that the Cu(II) nanoclusters act as electron trapping while the Ti(IV) nanoclusters act as hole trapping centers, respectively. Weak Ag signal appeared on the thin film surface, suggesting the adsorption of Ag species under the dark condition (Figure S28, Supporting Information).

The surface wetting behavior of the thin films was also investigated (Figure S29, Supporting Information), since the superhydrophilic conversion of TiO_2 is dominantly induced by photogenerated holes, which cause the surface reconstruction of hydroxyl groups.[62−64] Of the various thin films examined in the present study, the surface of Ti(IV)/TiO_2/Cu(II) became superhydrophilic under visible-light irradiation. These results confirmed that Ti(IV) nanoclusters are efficient hole trapping centers and are able to couple with electron trapping centers, such as Fe(III) and Cu(II) nanoclusters, for further enhancing the photocatalytic activity of TiO_2.

On the basis of these results, the proposed photocatalytic reaction mechanism of our photocatalysts is shown in Figure 5. Our experimental results clearly demonstrate that photogenerated electrons accumulate in Cu(II) and Fe(III) nanoclusters, while photogenerated holes accumulate in Ti(IV) nanoclusters on the surface of TiO_2. Under the visible light irradiation, electrons in the VB of TiO_2 can be transferred to surface Cu(II) or Fe(III) nanoclusters through an IFCT process[28,29] and efficiently consumed by multielectron reduction reactions, while the holes react hydroxyl groups to produce OH· radicals or directly react with organic contaminant.[30−33,59−61]

CONCLUSION

In summary, we have developed the efficient visible-light-active photocatalyt by the consideration of three requirements, *i.e.*, composed of ubiquitous elements, designed by novel clusters grafting, and produced by a facile fabrication process. Highly visible-light-active TiO_2 photocatalysts have been developed by the coupling of Ti(IV) and Fe(III) or Cu(II) nanoclusters on the surface. Ti(IV) nanoclusters were demonstrated to act as hole trapping centers on the surface of TiO_2 to efficiently oxidize organic contaminants, while Fe(III) or Cu(II) nanoclusters mediate the reduction of oxygen molecules under visible light irradiation. Therefore, our developed TiO_2 photocatalysts exhibited the highest QE of 92.2% and reaction rate (0.69 μmol/h) for IPA decomposition under visible-light irradiation (420−530 nm). The desirable properties of efficient photocatalytic performance with high stability under visible light with safe and ubiquitous elements composition enable these catalysts feasible for large-scale practical applications. Further, our research opens a strategic approach for developing efficient hole trapping centers on the semiconductors by grafting amorphous semicoductor nanoclusters and provide a simple and promising route for further improvment of the photocatalytic performances under visible light by coupling with hole trapping centers and electron trapping centers.

EXPERIMENTAL SECTION

Deposition of Ti(IV) Nanoclusters on TiO_2 Single Crystals. The grafting of Ti(IV) nanoclusters onto TiO_2 single crystals was performed using a impregnation method.[25] Briefly, (110)-oriented rutile TiO_2 single crystals (1 cm × 1 cm, around 0.22 g, Kougaku Giken, Japan) was first dispersed in 10 mL of distilled water. Titanium chloride ($TiCl_4$, Wako) was used as the Ti(IV) source and was diluted to 0.5 mol/L in a hydrochloride acid solution and water. The hydrochloride acid solution was used to suppress the hydrolysis of $TiCl_4$. The $TiCl_4$ solution was added to the aqueous TiO_2 suspension at a weight fraction of Ti relative to TiO_2 of 0.25 wt %. The resulting suspension was heated at 90 °C under stirring for 1 h. After the solution was cooled to room temperature naturally, the single crystals was washed thoroughly with distilled water and then dried at 110 °C for 24 h.

Preparation of Fe(III)−Ti(IV)−TiO_2 and Cu(II)−Ti(IV)−TiO_2 Powder Nanocomposites. Commercial TiO_2 (MT-150A, rutile phase, 15 nm grain size, 90 m^2/g specific surface area; Tayca Co.) was used as the starting material. To improve its crystallinity, TiO_2 was annealed at 950 °C for 3 h, and the calcined TiO_2 was then treated with 6 M HCl aqueous solution at 90 °C for 3 h under stirring. After filtration (0.025-μm membrane filter, Millipore), washing, and drying at 110 °C for 24 h, the resulting clear TiO_2 powder was used to prepare TiO_2 nanocomposites with grafted nanoclusters.

The grafting of Ti(IV) nanoclusters onto TiO_2 was performed using a similar impregnation method described above. The grafting of Fe(III) nanoclusters onto TiO_2 was performed using a similar impregnation method.[25] One gram of TiO_2 powder was first dispersed in 10 mL of distilled water. $FeCl_3 \cdot 6H_2O$ (Wako, 99.9%), acting as the source of Fe(III), was added to the aqueous TiO_2 suspension to give a weight fraction of Fe relative to TiO_2 of 0.05 wt %. The suspension was heated at 90 °C under stirring for 1 h. After the solution was cooled to room temperature naturally, the suspension was filtered twice through a 0.025-μm membrane filter (Millipore) and washed thoroughly with distilled water. The resulting residues were dried at 110 °C for 24 h and then ground into fine powder using an agate mortar and pestle. Cu(II)−Ti(IV)−TiO_2 nanocomposites were prepared

by a similar process using $CuCl_2 \cdot 2H_2O$ (Aldrich) in place of $FeCl_3 \cdot 6H_2O$.

Preparation of Ti(IV)/TiO_2/Cu(II) Thin Films. For the preparation of Ti(IV)/TiO_2/Cu(II) thin films, Cu(II) nanoclusters were first grafted on the quartz substrate by a similar impregnation method to that described above. $CuCl_2 \cdot 2H_2O$ (Aldrich) was used as the source of Cu(II). The quartz substrate was cleaned and immersed in an aqueous $CuCl_2$ solution containing Cu at a weight fraction to water of 0.01 wt %, which is equal to the concentration of the solution used in previous reports.[24] The substrate was heated in the aqueous $CuCl_2$ solution at 90 °C for 1 h. After the solution was cooled to room temperature naturally, the quartz substrate with grafted Cu(II) nanoclusters was washed gently with sufficient amounts of distilled water and was then dried at 110 °C for 24 h. TiO_2 thin films were deposited on the Cu(II) nanocluster-grafted quartz substrate using a spin-coating process. Commercial TiO_2 sol (*STS-01*, anatase, Ishihara Sangyo Co.) was used as the starting material and was spin coated on the quartz substrate at a velocity of 2000 rpm for 20 s.[52] The thin films were dried at 110 °C for 24 h. Finally, Ti(IV) nanoclusters were grafted on the TiO_2 thin films by a similar impregnation method.

Sample Characterization. The crystal structures of the prepared Fe(III)−Ti(IV)−TiO_2 and Cu(II)−Ti(IV)−TiO_2 samples were measured by powder X-ray diffraction (XRD) at room temperature on a Rigaku D/MAX25000 diffractometer with a copper target (λ = 1.54056 Å). UV−visible absorption spectra were recorded by the diffuse reflection method using a UV-2550 spectrometer (Shimadzu). Atomic force microscopy (AFM) and Kelvin probe force microscope (KPFM) measurements were carried out on an AFM instrument (SPM-9600, Shimadzu). A cantilever coated with Pt was used to obtain the surface potential data. The morphologies of the samples were investigated by scanning electron microscopy (SEM) using a Hitachi SU-8000 apparatus and transition electron microscopy (TEM) on a Hitachi HF-2000 instrument under an acceleration voltage of 200 kV. The specific surface areas of the samples were determined from the nitrogen absorption data at liquid nitrogen temperature using the Barrett−Emmett−Teller (BET) technique. The samples were degassed at 200 °C and the pressure was kept below 100 mTorr for a minimum of 2 h prior to analysis using a Micromeritics VacPrep 061 instrument. Electron spin resonance spectroscopy (ESR) measurements were performed at 77 K (liquid nitrogen) with a JEOL ES-RE2X ESR spectrometer under UV light irradiation (500 W mercury lamp (Ushio, USH 500D) with cut off filter below 380 nm). The surface compositions and depth profiles were studied by X-ray photoelectron spectroscopy (XPS) on an AXIS-ULTRA DLD spectrometer (Kratos Analytical, Ltd.). The binding energy data were calibrated with the C 1s signal at 284.5 eV. To obtain the XPS depth profile, the thin films were etched using an argon ion etcher at an acceleration voltage of 500 V. The argon ion etching time was 60 s for each cycle. After argon ion etching, the chamber was vacuumed to the pressure lower than 10^{-7} Pa, then the XPS analysis was started to detect the composition of the samples. Quantitative analysis was based on the peak intensity multiplied by sensitivity factors supplied by Kratos, which considered the geometric configuration of the apparatus. The depth profile analysis was repeated 50 cycles. XPS depth analysis has been conducted after the photo-oxidation of $Pb(NO_3)_2$ and photoreduction of $AgNO_3$ as described below.

Evaluation of Photocatalytic Properties. The activities of photocatalysts were evaluated by the decomposition of gaseous 2-propanol (IPA) under visible-light irradiation (420−530 nm) from a Xe lamp (LA-251Xe, Hayashi Tokei) equipped with glass filters (L-42, B-47, and C-40C, Asahi Techno-Glass). The light intensity was measured by a light radiometer (USR-45D, Ushio Co.) and set to 1.0 mW/cm^2. A 500 mL cylindrical glass vessel was used as the photocatalysis reactor. The experiments were performed according to the following procedure. First, 300 mg of photocatalyst powder was evenly spread on the bottom of a circular glass dish (area, 5.5 cm^2), which was mounted in the middle of the vessel reactor. The vessel was sealed with a rubber O-ring and a quartz cover, evacuated, and then filled with fresh synthetic air. To eliminate organic contaminants from the sample surface, the vessel was preilluminated with a Xe lamp (LA-251Xe, Hayashi Tokei Works) until the rate of CO_2 generation was less than 0.02 μmol/day. The vessel was evacuated and filled again with fresh synthetic air. The pressure inside the vessel was kept at about 1 atm. To begin the measurements, 300 ppmv (~6 μmol) of gaseous IPA was injected into the vessel. Prior to light irradiation, the vessel was kept in the dark to achieve the absorption/desorption equilibrium of IPA on the surfaces of photocatalysts. The IPA concentration first decreased and then remained constant, demonstrating the absorption/desorption equilibrium of IPA had been achieved. During this process, no acetone or CO_2 were detected under dark conditions, illustrating the IPA molecules were not decomposed by the photocatalysts under dark conditions. After equilibrium had been reached, the vessel was irradiated with visible light. During light irradiation, 1 mL gaseous samples were periodically extracted from the reaction vessel to monitor the concentrations of IPA, acetone, and CO_2 using a gas chromatograph (model GC-8A, Shimadzu Co., Ltd.).

Photo-oxidation of $Pb(NO_3)_2$ and Photoreduction of $AgNO_3$. The effects of nanoclusters on carrier trapping and separation were studied by measuring the photocatalytic oxidation of Pb^{2+} and reduction of Ag^+. For the analysis, 5 mL of 1 mM $Pb(NO_3)_2$ (Wako) or 1 mM $AgNO_3$ (Wako) solution and TiO_2 thin-films were placed in a glass reactor and kept in the dark for 1 h to reach adsorption−desorption equilibrium. The sample was then illuminated with visible-light (420−530 nm) generated from a Xe lamp (LA-251Xe, Hayashi Tokei) equipped with L-42, B-47, and C-40C glass filters (Asahi Techno-Glass). A spectro-radiometer (USR-45D, Ushio Co.) was employed to measure the visible-light intensity, which was adjusted to 1.0 mW cm^{-2}. The trapping of holes and electrons on the surface nanoclusters were monitored by two photochemical reactions: the oxidation of lead ions by photogenerated holes and the reduction of silver ions by photogenerated electrons, respectively. After irradiation for 1 h, thin-films were washed with water to remove the unreacted $AgNO_3$ or $Pb(NO_3)_2$. To investigate the position of deposited Ag or PbO_2 particles in thin films, XPS depth analysis was conducted.

Evaluation of Surface Wettability. The surface wettability, which relates to the self-cleaning properties of the TiO_2 photocatalyst, was evaluated by measurement of the water contact angle. The measurements were performed at room temperature using a commercial contact angle meter (CA-X, Kyowa Interface Science, Saitama, Japan). High-purity water was used for all measurements. Contact angle measurements were conducted at three points for each sample, and the experimental error for each point was within ±1 degree. Visible-light illumination (420−530 nm) was provided by a Xe lamp (LA-251Xe, Hayashi Tokei) equipped with glass filters (L-42, B-47, and C-40C, Asahi Techno-Glass). The light intensity was measured using a light radiometer (USR-45D, Ushio Co.) and set to 1.0 mW/cm^2.

Conflict of Interest: The authors declare no competing financial interest.

Acknowledgment. This work was performed under the management of the Project to Create Photocatalysts Industry for Recycling-Oriented Society supported by the New Energy and Industrial Technology Development Organization (NEDO) in Japan. This research was also supported by JST, PRESTO. We express gratitude to Dr. Z. Yan and Mr. G. Newton for the careful reading of the manuscript.

Supporting Information Available: Surface areas of samples, AFM images of Ti(IV) nanoclusters grafted TiO_2 single crystals, scheme for deposition of PbO_2 clusters on Ti(IV)−TiO_2 single crystals, ESR spectra, TEM images of Ti(IV)−TiO_2 nanocomposites, XRD patterns of Ti(IV)−TiO_2 nanocomposites, UV−visible spectra of Ti(IV) nanoclusters grafted anatase and rutile nanocomposites, CO_2 generation over Ti(IV) nanoclusters grafted anatase and rutile nanocomposites, scheme for preparation of Fe(III)−Ti(IV)−TiO_2 nanocomposites, XRD patterns, XPS spectra, SEM images, UV−visible spectra of Fe(III)−Ti(IV)−TiO_2 nanocomposites, XRD patterns, XPS spectra, SEM images, UV−visible spectra of Cu(II)−Ti(IV)−TiO_2 nanocomposites, light source for the visible light irradiation, CO_2 generation over and Cu(II)−Ti(IV)−TiO_2, process for QE calculation, photocatalytic activities of Fe(III)−Ti(IV)−TiO_2 and Cu(II)−Ti(IV)−TiO_2 with different

amount of Ti(IV) nanoclusters, stability test, scheme for preparation of Cu(II)/TiO_2/Cu(II) thin films, SEM images of Cu(II)/TiO_2/Cu(II) thin films, ESR spectra of Cu(II)−Ti(IV)−TiO_2 and Cu(II)−TiO_2 under visible light irradiation, Pb 4f and Ag 3d core-level spectra of Ti(IV)/TiO_2/Cu(II) and TiO_2/Cu(II) thin films after photodeposition, Ag 3d and Pb 4f core-level spectra of Ti(IV)/TiO_2/Cu(II) and TiO_2/Cu(II) thin films under dark condition, changes in water contact angle under visible-light irradiation. This material is available free of charge *via* the Internet at http://pubs.acs.org.

REFERENCES AND NOTES

1. Hoffmann, M. R.; Martin, S. T.; Choi, W. Y.; Bahnemann, D. W. Environmental Applications of Semiconductor Photocatalysis. *Chem. Rev.* **1995**, *95*, 69–96.
2. Chen, X.; Mao, S. S. Titanium Dioxide Nanomaterials: Synthesis, Properties, Modifications, and Applications. *Chem. Rev.* **2007**, *107*, 2891–2959.
3. Chen, X.; Shen, S.; Guo, L.; Mao, S. S. Semiconductor-Based Photocatalytic Hydrogen Generation. *Chem. Rev.* **2010**, *110*, 6503–6570.
4. Zhong, M.; Sato, Y.; Kurniawan, M.; Apostoluk, A.; Masenelli, B.; Maeda, E.; Ikuhara, Y.; Delaunay, J. J. ZnO Dense Nanowire Array on A Film Structure in A Single Crystal Domain Texture for Optical and Photoelectrochemical Applications. *Nanotechnology* **2012**, *23*, 495602.
5. Ohtani, B. Preparing Articles on Photocatalysis—Beyond the Illusions Misconceptions and Speculation. *Chem. Lett.* **2008**, *37*, 216–229.
6. Qu, Y. Q.; Duan, X. F. Progress, Challenge and Perspective of Heterogeneous Photocatalysts. *Chem. Soc. Rev.* **2013**, *42*, 2568–2580.
7. Fujishima, A.; Honda, K. Electrochemical Photolysis of Water at A Semiconductor Electrode. *Nature* **1972**, *238*, 37–38.
8. Linsebigler, A. L.; Lu, G. Q.; Yates, J. T. Photocatalysis on TiO_2 Surfaces: Principles, Mechanisms, and Selected Results. *Chem. Rev.* **1995**, *95*, 735–758.
9. O'Regan, B.; Gratzel, M. A Low-Cost, High-Efficiency Solar Cell Based on Dye-Sensitized Colloidal TiO_2 Films. *Nature* **1991**, *353*, 737–740.
10. Hashimoto, K.; Irie, H.; Fujishima, A. TiO_2 Photocatalysis: A Historical Overview and Future Prospects. *Jpn. J. Appl. Phys.* **2005**, *44*, 8269–8285.
11. Froschl, T.; Hormann, U.; Kubiak, P.; Kucerova, G.; Pfanzelt, M.; Weiss, C. K.; Behm, R. J.; Husing, N.; Kaiser, U.; Landfester, K.; *et al.* High Surface Area Crystalline Titanium Dioxide: Potential and Limits in Electrochemical Energy Storage and Catalysis. *Chem. Soc. Rev.* **2012**, *41*, 5313–5360.
12. Asahi, R.; Morikawa, T.; Ohwaki, T.; Aoki, K.; Taga, Y. Visible-Light Photocatalysis in Nitrogen-Doped Titanium Oxides. *Science* **2001**, *293*, 269–271.
13. Choi, W. Y.; Termin, A.; Hoffmann, M. R. The Role of Metal Ion Dopants in Quantum-Sized TiO_2: Correlation Between Photoreactivity and Charge Carrier Recombination Dynamics. *J. Phys. Chem.* **1994**, *98*, 13669–13679.
14. Yamashita, H.; Harada, M.; Misaka, J.; Takeuchi, M.; Ikeue, K.; Anpo, M. Degradation of Propanol Diluted in Water under Visible Light Irradiation Using Metal Ion-Implanted Titanium Dioxide Photocatalysts. *J. Photochem. Photobiol., A* **2002**, *148*, 257–261.
15. Sakthivel, S.; Kisch, H. Daylight Photocatalysis by Carbon-Modified Titanium Dioxide. *Angew. Chem., Int. Ed.* **2003**, *42*, 4908–4911.
16. Kamat, P. V.; Meisel, D. Nanoparticles in Advanced Oxidation Processes. *Curr. Opin. Colloid Interface Sci.* **2002**, *7*, 282–287.
17. Kudo, A.; Niishiro, R.; Iwase, A.; Kato, H. Effects of Doping of Metal Cations on Morphology, Activity, and Visible Light Response of Photocatalysts. *Chem. Phys.* **2007**, *339*, 104–110.
18. Kato, H.; Kudo, A. Visible-Light-Response and Photocatalytic Activities of TiO_2 and $SrTiO_3$ Photocatalysts Codoped with Antimony and Chromium. *J. Phys. Chem. B* **2002**, *106*, 5029–5034.
19. Miyauchi, M.; Takashio, M.; Tobimatsu, H. Photocatalytic Activity of $SrTiO_3$ Codoped with Nitrogen and Lanthanum under Visible Light Illumination. *Langmuir* **2004**, *20*, 232–236.
20. Mrowetz, M.; Balcerski, W.; Colussi, A. J.; Hoffmann, M. R. Oxidative Power of Nitrogen-Doped TiO_2 Photocatalysts under Visible Illumination. *J. Phys. Chem. B* **2004**, *108*, 17269–17273.
21. Irie, H.; Watanabe, Y.; Hashimoto, K. Nitrogen-Concentration Dependence on Photocatalytic Activity of $TiO_{2-x}N_x$ Powders. *J. Phys. Chem. B* **2003**, *107*, 5483–5486.
22. Kisch, H.; Zhang, L.; Lange, C.; Maier, W. F.; Antonius, C.; Meissner, D. Modified, Amorphous Titania-A Hybrid Semiconductor for Detoxification and Current Generation by Visible Light. *Angew. Chem., Int. Ed.* **1998**, *37*, 3034–3036.
23. Irie, H.; Miura, S.; Kamiya, K.; Hashimoto, K. Efficient Visible Light-Sensitive Photocatalysts: Grafting Cu(II) Ions onto TiO_2 and WO_3 Photocatalysts. *Chem. Phys. Lett.* **2008**, *457*, 202–205.
24. Irie, H.; Kamiya, K.; Shibanuma, T.; Miura, S.; Tryk, D. A.; Yokoyama, T.; Hashimoto, K. Visible Light-Sensitive Cu(II)-Grafted TiO_2 Photocatalysts: Activities and X-ray Absorption Fine Structure Analyses. *J. Phys. Chem. C* **2009**, *113*, 10761–10766.
25. Yu, H.; Irie, H.; Shimodaira, Y.; Hosogi, Y.; Kuroda, Y.; Miyauchi, M.; Hashimoto, K. An Efficient Visible-Light-Sensitive Fe(III)-Grafted TiO_2 Photocatalyst. *J. Phys. Chem. C* **2010**, *114*, 16481–16487.
26. Liu, M.; Qiu, X. Q.; Miyauchi, M.; Hashimoto, K. Cu(II) Oxide Amorphous Nanoclusters Grafted Ti^{3+} Self-Doped TiO_2: An Efficient Visible Light Photocatalyst. *Chem. Mater.* **2011**, *23*, 5282–5286.
27. Liu, M.; Qiu, X. Q.; Miyauchi, M.; Hashimoto, K. Energy-Level Matching of Fe (III) Ions Grafted at Surface and Doped in Bulk for Efficient Visible-Light Photocatalysts. *J. Am. Chem. Soc.* **2013**, *135*, 10064–10072.
28. Creutz, C.; Brunschwig, B. S.; Sutin, N. Interfacial Charge Transfer Absorption: Semiclassical Treatment. *J. Phys. Chem. B* **2005**, *109*, 10251–10260.
29. Creutz, C.; Brunschwig, B. S.; Sutin, N. Interfacial Charge-Transfer Absorption: 3. Application to Semiconductor-Molecule Assemblies. *J. Phys. Chem. B* **2006**, *110*, 25181–25190.
30. Himo, F.; Eriksson, L. A.; Maseras, F.; Siegbahn, P. E. M. Catalytic Mechanism of Galactose Oxidase: A Theoretical Study. *J. Am. Chem. Soc.* **2000**, *122*, 8031–8036.
31. Goldstein, S.; Czapski, G.; Eldik, R.; Cohen, H.; Meyerstein, D. Determination of The Volume of Activation of The Key Reaction Steps in The Oxidation of Phenanthroline-Copper(I) by Molecular Oxygen. *J. Phys. Chem.* **1991**, *95*, 1282–1285.
32. Kitajima, N.; Morooka, Y. Copper-Dioxygen Complexes. Inorganic and Bioinorganic Perspectives. *Chem. Rev.* **1994**, *94*, 737–757.
33. Cole, A. P.; Root, D. E.; Mukherjee, P.; Solomon, E. I.; Stack, T. D. P. A Trinuclear Intermediate in The Copper-Mediated Reduction of O_2: Four Electrons from Three Coppers. *Science* **1996**, *273*, 1848–1850.
34. Nosaka, Y.; Takahashi, S.; Sakamoto, H.; Nosaka, A. Reaction Mechanism of Cu(II)-Grafted Visible-Light Responsive TiO_2 and WO_3 Photocatalysts Studied by Means of ESR Spectroscopy and Chemiluminescence Photometry. *J. Phys. Chem. C* **2011**, *115*, 21283–21290.
35. Nishikawa, M.; Mitani, Y.; Nosaka, Y. Photocatalytic Reaction Mechanism of Fe(III)-Grafted TiO_2 Studied by Means of ESR Spectroscopy and Chemiluminescence Photometry. *J. Phys. Chem. C* **2012**, *116*, 14900–14907.
36. Kudo, A.; Miseki, Y. Heterogeneous Photocatalyst Materials for Water Splitting. *Chem. Soc. Rev.* **2009**, *38*, 253–278.
37. Maeda, K.; Domen, K. Photocatalytic Water Splitting: Recent Progress and Future Challenges. *J. Phys. Chem. Lett.* **2010**, *1*, 2655–2661.
38. Yang, J. H.; Wang, D. E.; Han, H. X.; Li, C. Roles of Cocatalysts in Photocatalysis and Photoelectrocatalysis. *Acc. Chem. Res.* **2013**, *46*, 1900–1909.

39. Lin, F.; Wang, D.; Jiang, Z.; Ma, Y.; Li, J.; Li, R.; Li, C. Photocatalytic H_2 Production on $Pt/TiO_2-SO_4^{2-}$ with Tuned Surface-Phase Structures: Enhancing Activity and Reducing CO Formation. *Energy Environ. Sci.* **2012**, *5*, 6345–63351.
40. Meekins, B. H.; Kamat, P. V. Role of Water Oxidation Catalyst IrO_2 in Shuttling Photogenerated Holes Across TiO_2 Interface. *J. Phys. Chem. Lett.* **2011**, *2*, 2304–2310.
41. Yang, J.; Yan, H.; Wang, X.; Wen, F.; Wang, Z.; Fan, D.; Shi, J.; Li, C. Roles of Cocatalysts in Pt−PdS/CdS with Exceptionally High Quantum Efficiency for Photocatalytic Hydrogen Production. *J. Catal.* **2012**, *290*, 151–157.
42. Maeda, K.; Xiong, A.; Yoshinaga, T.; Ikeda, T.; Sakamoto, N.; Hisatomi, T.; Takashima, M.; Lu, D.; Kanehara, M.; Setoyama, T.; *et al.* Photocatalytic Overall Water Splitting Promoted by Two Different Cocatalysts for Hydrogen and Oxygen Evolution under Visible Light. *Angew. Chem., Int. Ed.* **2010**, *49*, 4096–4099.
43. Ma, S.; Maeda, K.; Abe, R.; Domen, K. Visible-Light-Driven Nonsacrificial Water Oxidation over Tungsten Trioxide Powder Modified with Two Different Cocatalysts. *Energy Environ. Sci.* **2012**, *5*, 8390–8397.
44. Wang, D.; Hisatomi, T.; Takata, T.; Pan, C.; Katayama, M.; Kubota, J.; Domen, K. Core/Shell Photocatalyst with Spatially Separated Co-catalysts for Efficient Reduction and Oxidation of Water. *Angew. Chem., Int. Ed.* **2013**, *52*, 11252–11256.
45. Kana, M. W.; Nocera, D. G. *In Situ* Formation of An Oxygen-Evolving Catalyst in Neutral Water Containing Phosphate and Co^{2+}. *Science* **2008**, *321*, 1072–1075.
46. Hosono, H.; Hayashi, K.; Kamiya, T.; Atou, T.; Susaki, T. New Functionalities in Abundant Element Oxides: Ubiquitous Element Strategy. *Sci. Technol. Adv. Mater.* **2011**, *12*, 034303.
47. Iwaszuk, A.; Nolan, M. Reactivity of Sub 1 nm Supported Clusters: $(TiO_2)_n$ Clusters Supported on Rutile TiO_2 (110). *Phys. Chem. Chem. Phys.* **2011**, *13*, 4963–4973.
48. Gopal, N. O.; Lo, H. H.; Sheu, S. C.; Ke, S. C. A Potential Site for Trapping Photogenerated Holes on Rutile TiO_2 Surface as Revealed by EPR Spectroscopy: An Avenue for Enhancing Photocatalytic Activity. *J. Am. Chem. Soc.* **2010**, *132*, 10982–10983.
49. Melitz, W.; Shen, J.; Kummel, A. C.; Lee, S. Kelvin Probe Force Microscopy and Its Application. *Surf. Sci. Rep.* **2011**, *66*, 1–27.
50. Barth, C.; Foster, A. S.; Henry, C. R.; Shluger, A. L. Recent Trends in Surface Characterization and Chemistry with High-Resolution Scanning Force Methods. *Adv. Mater.* **2011**, *23*, 477–501.
51. Kokawa, R.; Ohta, M.; Sasahara, A.; Onishi, H. Kelvin Probe Force Microscopy Study of a Pt/TiO_2 Catalyst Model Placed in An Atmospheric Pressure of N_2 Environment. *Chem.—Asian J.* **2012**, *7*, 1251–1255.
52. Anandan, S.; Miyauchi, M. Improved Photocatalytic Efficiency of A WO_3 System by An Efficient Visible-Light Induced Hole Transfer. *Chem. Commun.* **2012**, *48*, 4323–4325.
53. Hermann, J. M.; Disdier, J.; Pichat, P. Photocatalytic Deposition of Silver on Powder Titania: Consequences for The Recovery of Silver. *J. Catal.* **1988**, *113*, 72–81.
54. Ohno, T.; Sarukawa, K.; Matsumura, M. Crystal Faces of Rutile and Anatase TiO_2 Particles and Their Roles in Photocatalytic Reactions. *New J. Chem.* **2002**, *26*, 1167–1170.
55. Nakaoka, Y.; Nosaka, Y. ESR Investigation into The Effects of Heat Treatment and Crystal Structure on Radicals Produced over Irradiated TiO_2 Powder. *J. Photochem. Photobiol., A* **1997**, *110*, 299–305.
56. Micic, O. I.; Zhang, Y.; Cromack, K. R.; Trifunac, A. D.; Thurnauer, M. C. Trapped Holes on Titania Colloids Studied by Electron Paramagnetic Resonance. *J. Phys. Chem.* **1993**, *97*, 7277–7283.
57. Hurum, D. C.; Agrios, A. G.; Crist, S. E.; Gray, K. A.; Rajh, T.; Thyrnauer, M. C. Probing Reaction Mechanisms in Mixed Phase TiO_2 by EPR. *J. Electron Spectrosc. Relat. Phenom.* **2006**, *150*, 155–163.
58. Coronado, J. M.; Maira, A. J.; Conesa, J. C.; Yeung, K. L.; Augugliaro, V.; Soria, J. EPR Study of The Surface Characteristics of Nanostructured TiO_2 under UV Irradiation. *Langmuir* **2001**, *17*, 5368–5374.
59. Kumar, C. P.; Gopal, N. O.; Wang, T. C.; Wong, M. S.; Ke, S. C. EPR Investigation of TiO_2 Nanoparticles with Temperature-Dependent Properties. *J. Phys. Chem. B* **2006**, *110*, 5223–5229.
60. Brezova, V.; Stasko, A.; Lapcik, L., Jr. Electron Paramagnetic Resonance Study of Photogenerated Radicals in Titanium Dioxide Powder and Its Aqueous Suspensions. *J. Photochem. Photobiol., A* **1991**, *59*, 115–121.
61. Jaeger, C. D.; Bard, A. J. Spin Trapping and Electron Spin Resonance Detection of Radical Intermediates in The Photodecomposition of Water at Titanium Dioxide Particulate Systems. *J. Phys. Chem.* **1979**, *83*, 3146–3152.
62. Wang, R.; Hashimoto, K.; Fujishima, A.; Chikuni, M.; Kojima, E.; Kitamura, A.; Shimohigoshi, M.; Watanabe, T. Light-Induced Amphiphilic Surfaces. *Nature* **1997**, *388*, 431–432.
63. Wang, R.; Hashimoto, K.; Fujishima, A.; Chikuni, M.; Kojima, E.; Kitamura, A.; Shimohigoshi, M.; Watanabe, T. Photogeneration of Highly Amphiphilic TiO_2 Surfaces. *Adv. Mater.* **1998**, *10*, 135–138.
64. Carp, O.; Huisman, C. L.; Reller, A. Photoinduced Reactivity of Titanium Dioxide. *Prog. Solid State Chem.* **2004**, *32*, 33–177.